Cell Reports, Volume *23*

Supplemental Information

Molecular and Functional Sex Differences of Noradrenergic Neurons in the Mouse Locus Coeruleus

Bernard Mulvey, Dionnet L. Bhatti, Sandeep Gyawali, Allison M. Lake, Skirmantas Kriaucionis, Christopher P. Ford, Michael R. Bruchas, Nathaniel Heintz, and Joseph D. Dougherty

Supplemental Material

Included contents:

Figs. S1 to S5 and legends
Table S2 and legend
Supplemental Experimental Procedures
Supplemental References

See also:

Table S1 (separate .xls file with 9 sheets: 1a-1k)
Table S3 (separate .xls file with 1 sheet)

Supplemental Figures S1-S5: (*beginning on next page*)

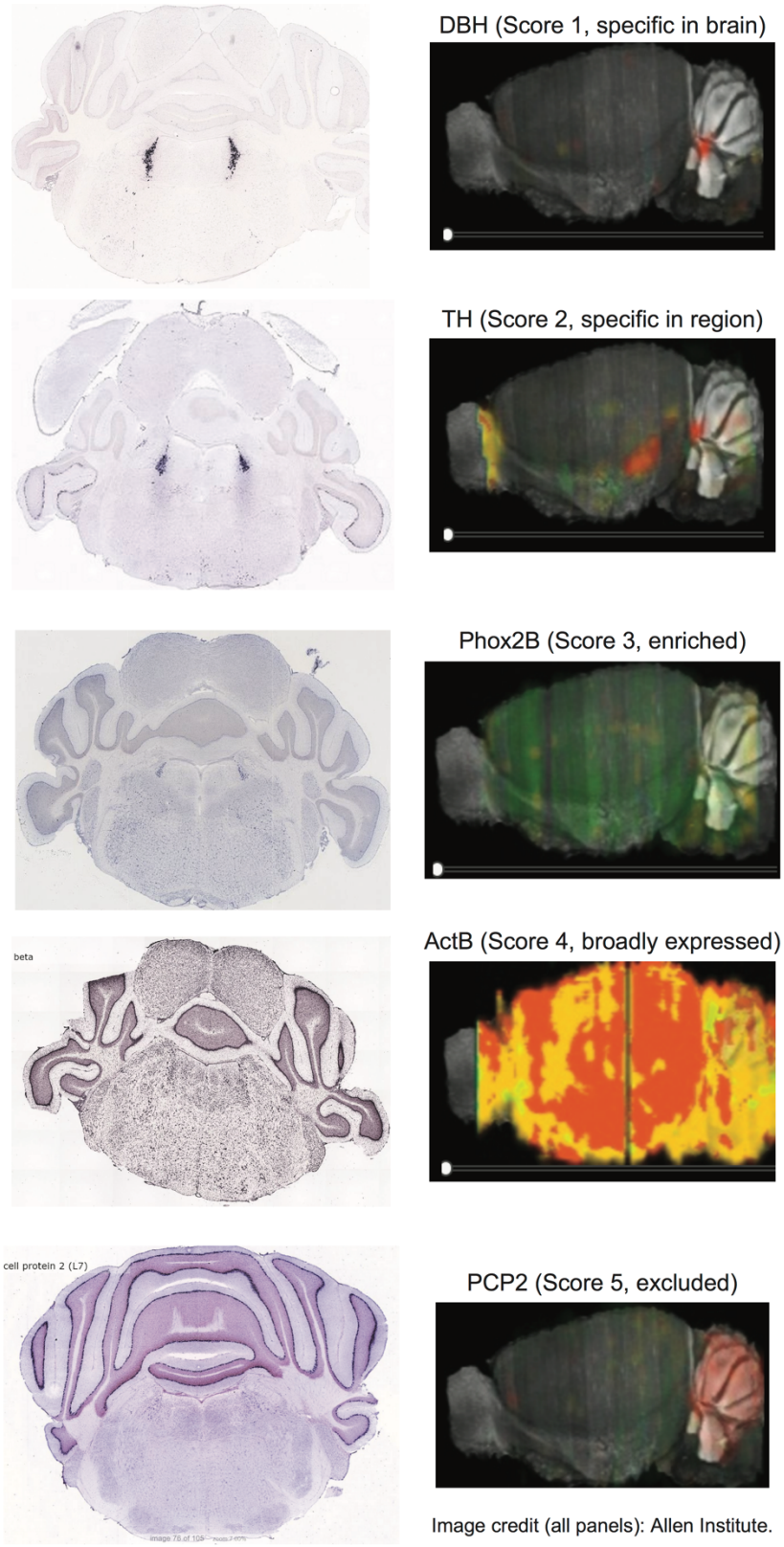

Fig. S1: Examples of Allen Brain Atlas In Situ Hybridizations scored 1-5. Related to Figure 2. Images from Allen Brain Atlas for examples of *in situ* hybridizations that would score a 1-5, respectively. Images of whole sections stitched from higher magnification images.

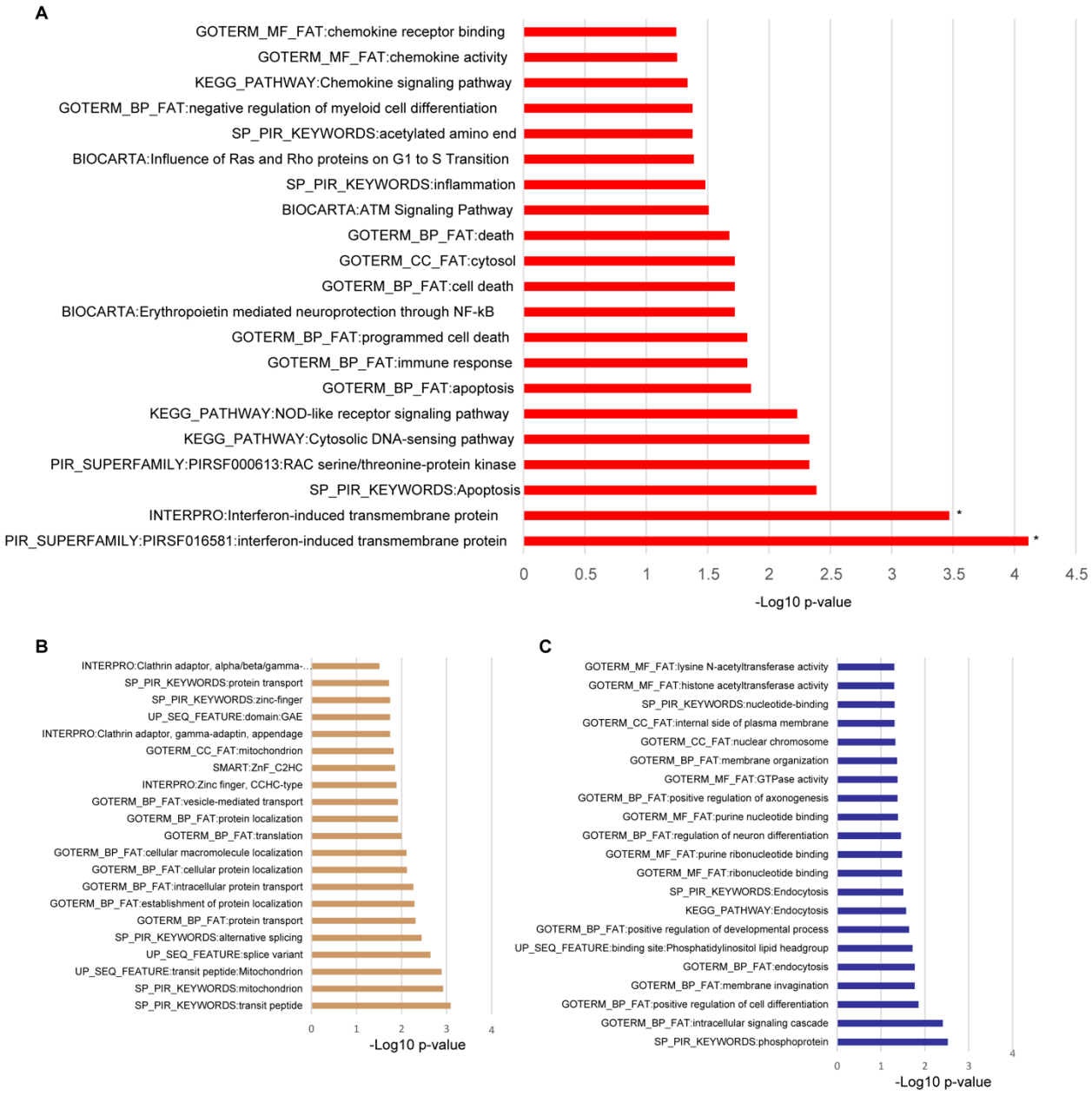

Figure S2: Pathway analysis of transcripts altered in hindbrain by LPS and of sex-differentially expressed transcripts in noradrenergic neurons. Related to Figure 3. A) A pathway analysis using DAVID reveals the hindbrain showed a significant increase of interferon related gene expression, and trends in a variety of chemokine and inflammatory pathways. B,C) An exploratory pathway analysis using DAVID illustrates the trends in male and female noradrenergic gene lists (*-Log10 p-values. No p<0.05 after Benjamini-Hochberg correction for multiple testing).* Though no individual pathway survived correction for multiple testing, the trend towards more mitochondrial genes and vesicular transport transcripts in female neurons may suggest they have slightly higher metabolic demands. Male neurons had slightly more nuclear factors, driven by transcription factors such as *Atrx1*, *Mtf1* and *Pbx1*.

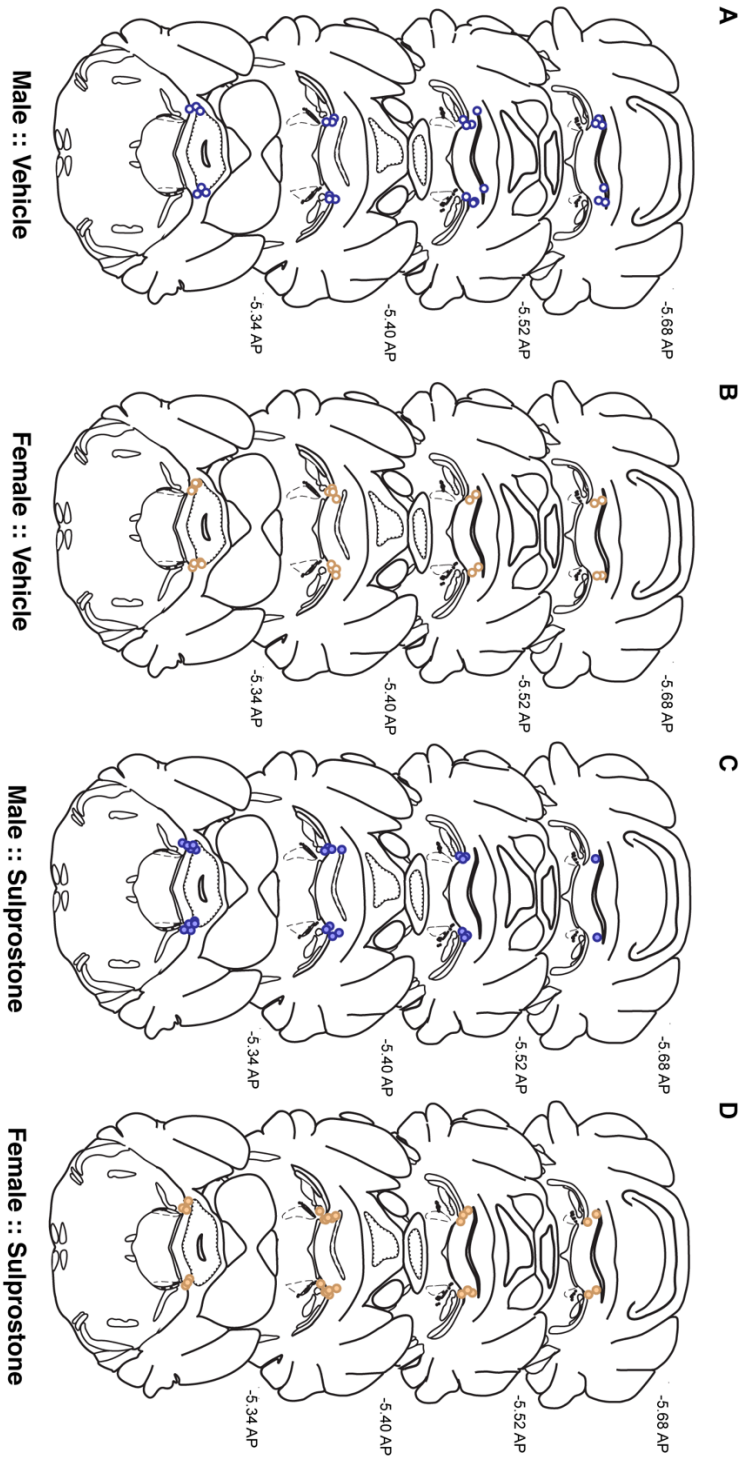

Figure S3: Map of LC cannula placements from post-mortem brain tissue. Related to Experimental Procedures. Tissue from all mice cannulated and given sulprostone or vehicle was sliced, and the deepest point of the two cannula tracks was noted for each mouse. These points are collectively mapped here for mice across all conditions. If cannulae were not in the target area, the mice/tissue were excluded from behavioral analysis, c-FOS quantification, and this diagram. Anatomy is shown in the coronal plane with mm along anterior-posterior (AP) axis;

dotted lines outline location of the LC. Circle outlines: blue = male, orange = female; fill color: purple = sulprostone-treated, empty/white = vehicle-treated.

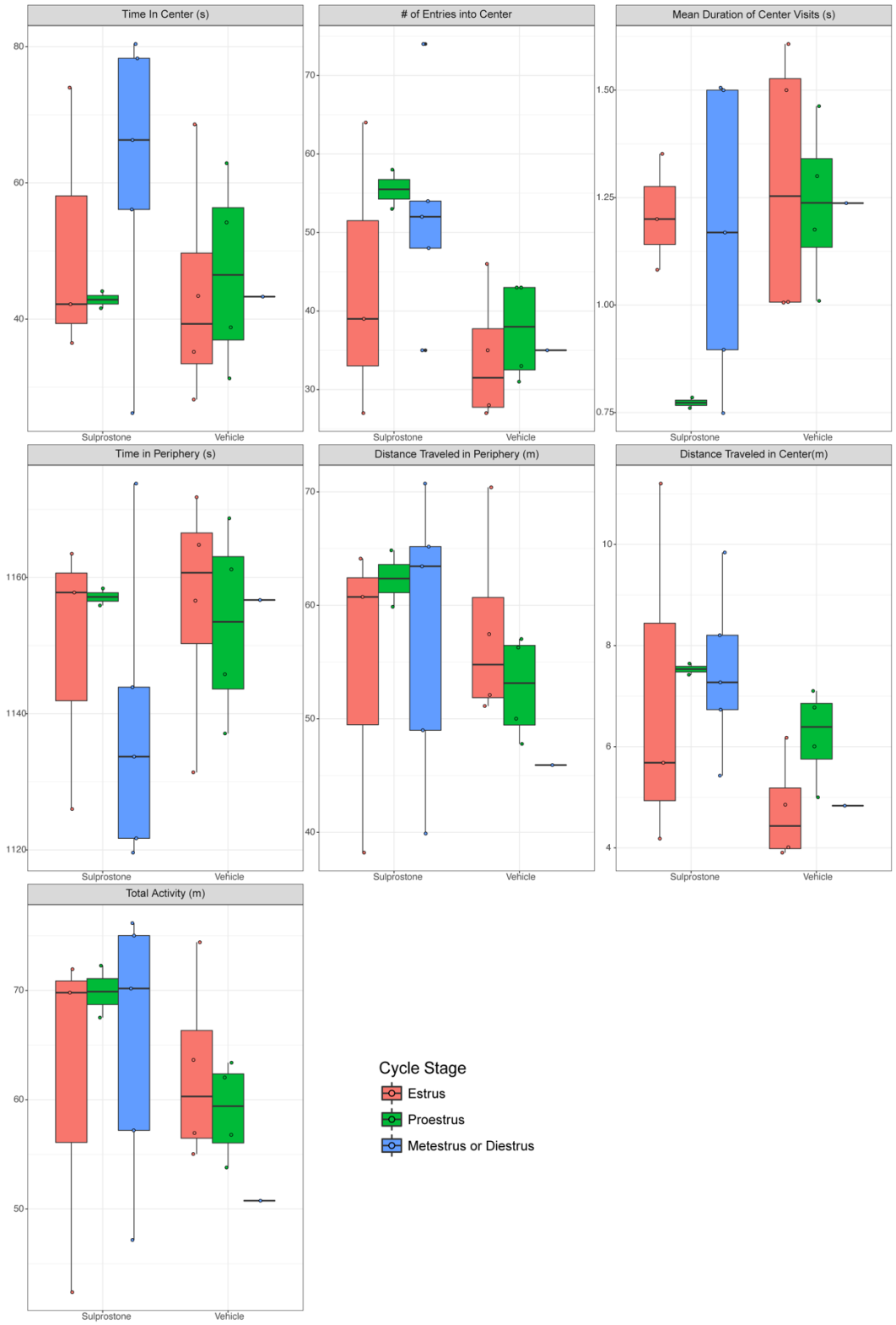

Figure S4: OFT data by estrus stage from one cohort of sulprostone-behavior mice. Related to Figure 4. Boxplots for seven OFT measures in counts, meters (m), or seconds (s) from females in a cohort of sulprostone-behavior mice with estrus staging data. Bottom and top of boxes represent 25th and 75th percentiles, respectively;

line inside the box represents the median (50th percentile), and individual points represent outliers. Metestrus and diestrus were combined per (Silva et al., 2016).

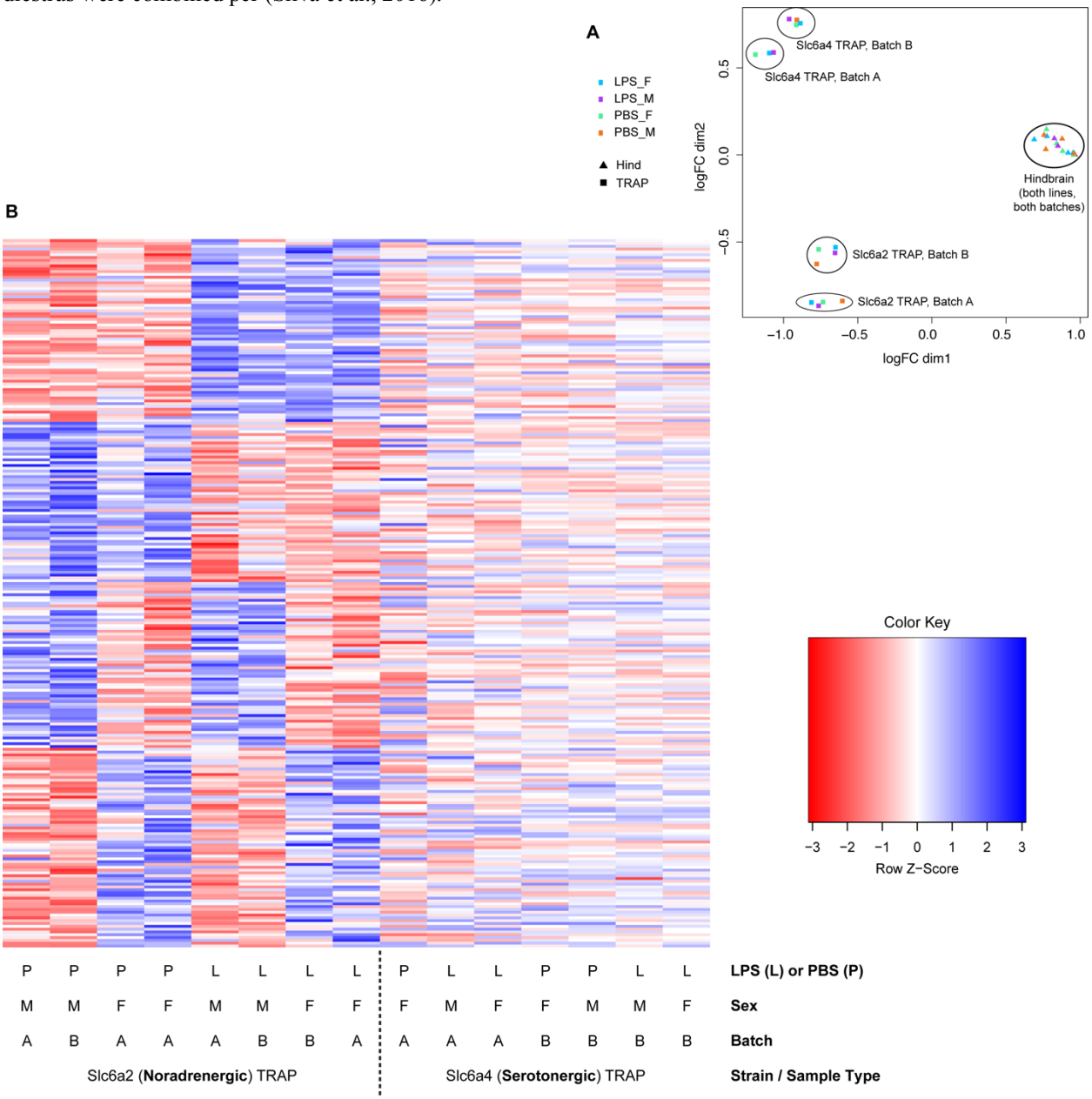

Figure S5: Multidimensional scaling (MDS) and heatmaps illustrate the clustering of samples and gene sets. Related to Figures 1-3 and Experimental Procedures. A) Hierarchical clustering confirms the expected segregation of samples by cell/sample type (*Slc6a2* vs. *Slc6a4* vs. hindbrain, or TRAP vs. hindbrain), and show a degree of batch effects, guiding the analytical strategies employed. B) Clustering genes that were DE between at least one comparison in the *Slc6a2* TRAP samples (i.e., comparing expression between sexes or between LPS/PBS conditions) illustrates the presence of distinct LPS-and sex-dependent DEG sets in noradrenergic neurons. The adjacent *Slc6a4* samples illustrate that sex and LPS do not affect these genes in serotonergic neurons in an analogous manner.

Motif	Total # motif occurrences found	# of unique sequences matching	E-value	Chi-sq p-value (vs. 1,000 random)	Select TFBS Predictions (TomTom)	Sequence
Female LC-Enriched TSS regions						
Fz4	26	26 / 77	1.7E-58	4.59E-03	NR4A2, NR2F6, OTX2	
Fz9**	19	19 / 77	2.7E-24	3.60E-11	(None)	
Fz10	13	13 / 77	3.4E-21	0.5518	OTX2	
Fa4	37	22 / 77	8.0E-97	0.1426	OTX2	
Fa10**	22	17 / 77	1.1E-41	8.28E-13	FOS, FOS::JUN, TBX1, MAZ	
Fa12**	31	19 / 77	6.3E-63	5.43E-07	(None)	
Male LC-Enriched TSS regions						
Mz1	15	15 / 70	1.5E-46	0.5645	(None)	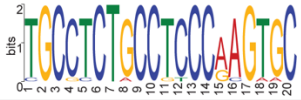
Mz2**	20	20 / 70	1.5E-19	4.50E-04	MTF1, OTX2	
Ma3*	31	24 / 70	2.1E-104	5.17E-03	NR2F6, OTX2	
Ma4*	23	18 / 70	3.1E-61	0.0198	OTX2	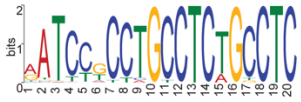
Mvf1	13	13 / 70	1.0E-44	1.00	Let-7, NR2F6, MAZ	
Mvf3	11	11 / 70	2.1E-07	0.1531	(None)	

Table S2: Motifs discovered in conserved, noncoding regions near sex-DEGs. Related to Experimental Procedures.

Motif: Refers to the sex, algorithm (allowing ≤ 1 or ≥ 1 motif occurrence per query sequence) and the result # in the MEME output. *Total # motif occurrences found:* total number of significant matches for the motif. *# Unique sequences matching:* the number of queried sequences with ≥ 1 motif match out of the total number of sequences queried. *E-value*: a MEME measure of probability compared to a shuffled version of the input sequences. *Chi-sq p value*: from comparative abundance of the identified motif in 1,000 randomly selected, protein-coding gene regions subjected to the same masking paradigm. *Select TFBS predictions*: TFBSes identified using TomTom with previously described expression in neural cell types and of functional and/or cell type relevance to the LC. *Sequence*: the position-weight matrix (PWM) given in the MEME results.

Supplemental Experimental Procedures

Animal Research Statement

All procedures involving animals were approved by the Institutional Animal Care and Use Committees of Rockefeller University, Case Western Reserve University, and Washington University in St. Louis.

Generation of LC TRAP mice and selection of an LC-specific TRAP mouse line. We initially modified BACs to be controlled by the promoters of either of two genes with LC-specific expression: Dopamine Beta Hydroxylase (*Dbh,* BAC RP23-354N13)*,* involved in the synthesis of NE (*16*), and the NE reuptake transporter (*Slc6a2,* RP23-109O23) (*17*). BACs were modified as described (Doyle et al., 2008) to insert the TRAP transgene (EGFP/Rpl10a) at the translation start site of the relevant gene. Successful modification was confirmed with Southern blot, and the absence of gross rearrangements in the BACs was verified by BAC fingerprinting and pulse field gel. Modified BAC DNA was purified with CsCl gradient centrifugation, dialyzed into injection buffer, and injected into FVB mouse eggs. Eggs were transplanted into pseudo-pregnant Swiss Webster dams; tail tips of the resultant pups were PCR genotyped for EGFP to identify founders. Founders were crossed to C57/BL6J wildtype mice, whose F1 progeny were genotyped and processed for anatomy as described below. Multiple founder lines were evaluated for EGFP expression; lines from both *Dbh* and *Slc6a2* constructs showed EGFP/Rpl10a expression in the LC and other noradrenergic populations. The lines for *Slc6a2* consistently demonstrated more robust EGFP/Rpl10a expression—as described in the main text's results section and **Figure 1**—and were thus selected for complete anatomical and biochemical evaluation. Two of the *Slc6a2* founders were used for initial transcriptional profiling (these lines were delegated B6;FVB-Tg (*Slc6a2*-EGFP/Rpl10a)JD1537$^{Jdd/J}$ and B6;FVB-Tg (*Slc6a2*-EGFP/Rpl10a)JD1538$^{Jdd/J}$) (**Figure 1E**, **2A**). The line JD1538 was further used to contrast transcriptional profiles of LC under different fixed and environmental conditions (sex and LPS injection) (**Figure 3**).

Immunofluorescence microscopy. Mice were sacrificed then perfused with phosphate buffered saline (PBS) followed by 4% paraformaldehyde in PBS. Brains were dissected, cryoprotected in 30% sucrose PBS solution, frozen, and sectioned serially on a Leica cryostat into PBS with 0.1% sodium azide for storage at 4°C. Floating sections were incubated at room temperature for 30 minutes in a blocking buffer of 5% normal donkey serum and 0.25% Triton in PBS followed by overnight incubation with primary antibodies in blocking buffer. Sections were washed 3 times with PBS, then incubated for 60-90 minutes with appropriate Alexa fluorophore-conjugated secondary antibodies and nuclear dye (DAPI or TOPO-3-Iodide, *Life Technologies*). Images were acquired on a LSM 510 Zeiss confocal microscope or a Perkin Elmer UltraView Vox spinning disk confocal via a Zeiss Axiovert microscope. Antibodies used are described in **Table S1j**.

Immunohistochemistry. Mice were processed as above. For anti-GFP DAB immunohistochemistry, brains were processed utilizing multibrain technology by Neuroscience Associates (*Knoxville, TN)* as described (Doyle et al., 2008), using a custom goat anti-GFP antibody and a Nickel enhanced DAB substrate for HRP. Sections were digitized with a Zeiss Axioskop2 using customized macros.

In-situ *hybridization (ISH) for detection of Calcr mRNA*. Two adult (P>60) C57BL/6J male littermates and one P35 male FVB-Ant mouse were sacrificed by CO_2 asphyxiation. Brains were transferred to cryoprotectant, and stored at -80°C for <4 weeks. 20µm cryosections were cut and directly mounted onto slides for ISH. The antisense *Calcr* probe region was selected to complement a constitutive exon. The probe was amplified by PCR with primers containing an appropriately-oriented T7 polymerase promoter, and probes were subsequently synthesized by *in vitro* transcription (per mfg. instructions) using T7 polymerase (*Promega #P2075*) and Digoxigenin RNA Labeling Mix (*Roche #11277073910*). For ISH, slides were incubated in 4% paraformaldehyde for 10min to fix tissue. Probe was hybridized to slides in a humid chamber at 68°C overnight and washed. Alkaline phosphatase-coupled anti-digoxigenin antibodies (**Table S1j**) were used for detection (4°C overnight incubation), followed by staining with NBT and BCIP, resulting in black staining by alkaline phosphatase. Primers for the *Calcr* probe were: 5' GCCAGTGGACGCAGTTCAAGATCCAGTGG 3' and 5' **gcacgTAATACGAC-TCACTATAG**GCCTGCTTTCCTACGAACACAGTCATCTCAGTCC 3' (in bold lowercase: bases added to end to allow room for T7 association, per mfg. instructions; in bold uppercase, the T7 promoter).

TRAP for initial description of LC. Replicate pools of five mixed sex adult mice from each of the *Slc6a2* lines were sacrificed. Brains were removed and transferred to ice-cold dissection buffer containing cycloheximide for collection of hindbrain posterior to the pontine/hypothalamic junction (discarding the cerebellum). TRAP was conducted as described (Doyle et al., 2008). Briefly, each pooled sample of hindbrains was homogenized in buffer

(10 mM HEPES [pH 7.4], 150 mM KCl, 5 mM $MgCl_2$, 0.5 mM dithiothreitol, 100 µg/ml cycloheximide, protease inhibitors, and recombinant RNase inhibitors) using a glass teflon homogenizer on ice. Nuclei and debris were removed with centrifugation at 2000 x *g* for 10 min at 4°C. DHPC (Avanti, Alabastar, AL) and NP-40 (Ipgal-ca630, Sigma, St Louis, MO) were added to the supernatant (final concentrations of 30mM and 1%, respectively) and incubated on ice for 5 minutes. This supernatant was centrifuged at 20,000 x *g* for 15 minutes at 4°C, and pellet was discarded. Protein G-coated magnetic beads (Invitrogen/Life Technologies, Grand Island, NY), conjugated to a mix of two monoclonal anti-GFP antibodies (Doyle et al., 2008), and incubated with supernatant by rotation for 30 minutes at 4°C. Beads were washed three times with high salt wash buffer (10 mM HEPES [pH 7.4], 350 mM KCl, 5 mM $MgCl_2$, 1% NP-40, 0.5 mM dithiothreitol, and 100 µg/ml cycloheximide). RNA was purified from ribosomes using Trizol (Invitrogen), followed by DNAse treatment, further purification, and concentration with RNeasy MinElute columns (*Qiagen, Hilden, Germany*) according to the manufacturers' protocols. RNA was also harvested in parallel from each unbound fraction of affinity purification as a measure of total hindbrain RNA. RNA concentration of all samples was measured with Nanodrop spectrophotometer and integrity (RIN>8) was confirmed with PicoChips on the Agilent BioAnalyzer.

Each RNA sample was amplified with the Affymetrix Two-Cycle amplification kit per manufacturer's instructions. Quality of labeled aRNA was assessed with Bioanalyzer. aRNAs from immunoprecipitated ribosomes and total tissue were hybridized to separate Affymetrix Mouse Genome 430 2.0 arrays and scanned following manufacturer protocols. Raw data are available from the Gene Expression Omnibus (GEO): **GSE100005.**

Data were analyzed using the Bioconductor module within the R programming language. Data were normalized as described (Dougherty et al., 2010). Briefly, GCRMA was used to normalize within replicates, and to biotinylated spike in probes (green dots, **Figure 1F**) between conditions. Fold change, Specificity Index (SI) and pSI were calculated for all genes with expression above non-specific background, and >50 arbitrary fluorescent units, as described (Dougherty et al., 2010). The threshold to identify genes expressed above background was conservatively set at the mean plus 2 standard deviations of the fold change of negative control transcripts comparing the TRAP samples to hindbrain mRNA (**Figure 1F**, red dots). Genes with expression below this level may or may not be found in LC neurons. To identify transcripts enriched in LC neurons compared to hindbrain RNA, we utilized the empirical Bayesian statistic with FDR correction within the *l*imma package. Positive control transcripts plotted in **Figure 1** include genes with known specificity and functionality in LC: *Th (Austin et al., 1990; Bacopoulos and Bhatnagar, 1977), Ddc* (Weihe et al., 2006), *Maoa (Hasegawa et al., 1999)*, *Dbh* (Swanson and Hartman, 1975), *Slc18a2* (Weihe et al., 2006)*, Slc6a2*, *Gal, GalR1* (Melander et al., 1986), and *Phox2a* (Morin et al., 1997). We used the pSI algorithm with default settings to compare the LC expression profile with other mouse brain cell populations characterized by TRAP (Dalal et al., 2013; Dougherty et al., 2013; Doyle et al., 2008; Görlich et al., 2013; Xu et al., 2014). Cell types included in this analysis are listed in **Figure 1G**. Hierarchical clustering across cell types was conducted in R utilizing expression values from genes with pSI <0.01 in any cell type. Finally, Gene Ontologies analysis throughout the manuscript was conducted with the DAVID interface's Functional Annotation Chart tool (Dennis et al., 2003).

Single animal TRAP for sex-differential and LPS-responsive gene expression. Four adult male and four adult female mice from each of the bacTRAP lines (B6;FVB-Tg (*Slc6a4*-EGFP/Rpl10a)JD60$^{Htz/J}$ (Dougherty et al., 2013), and B6;FVB-Tg (*Slc6a2*-EGFP/Rpl10a)JD1538$^{Jdd/J}$) were surgically implanted with peritoneal G2 E-Mitter Transponders (*Phillips Respironics*), then single-housed for 48 hours to allow continuous telemetric monitoring of temperature and activity using the Vital View software and ER-4000 Energizer Receivers. Housing was maintained at 30°C (thermoneutral for a mouse) to permit induction of fever (Chai et al., 1996; Gordon, 1993; Kozak et al., 1998; Leon, 2002). On the day of the experiment, mice were injected at 07:30 AM intraperitoneally with 100 ug/kg of LPS (Sigma 0111:B4) or vehicle (sterile PBS) and monitored for lethargy and induction of fever with telemetery. Pilot experiments in a separate cohort established that fever peaked around 14:00. Experimental mice were euthanized at 14:00-14:30, at which point mice displayed substantial lethargy and a mean fever of 2.175°C ± 1.18 (SD) above preceding minimal body temperature. Hindbrains were dissected and processed for TRAP as described (Heiman et al., 2014). RNA quality was checked as above and quantified with Ribogreen assay. 3-7 ng per sample were amplified with Nugen Ovation PicoSL and hybridized to Illumina Mouse WG6 microarrays. Samples were handled and hybridized in two batches counterbalanced for mouse line, sex, and LPS exposure. Data were analyzed using Bioconductor/R. Examination of distribution of expression levels led to the exclusion of one *Slc6a4* TRAP sample and two hindbrain samples for poor hybridization. Remaining TRAP and hindbrain samples were separately normalized using the lumi package. Appropriate clustering of replicates was confirmed with multidimensional

scaling (MDS) (**Figure S5**). TRAP samples were again compared to hindbrain mRNAs, which confirmed TRAP enrichment of markers for each respective cell type. Only genes with TRAP/hindbrain expression above glial background (Dougherty et al., 2010) (>0.85 here), and absolute expression >200 fluorescent units were included for downstream expression comparisons (sex or LPS/PBS). For each mouse line, probes were defined as differentially expressed if p<.05 on a paired T-test (pairing by experimental batch and covariate) and Log2 change was +/- .585 (1.5 fold) across 3 of 4 paired comparisons. For balance purposes, the remaining replicate was used twice to replace the low quality excluded *Slc6a4* TRAP sample. Results of these analyses are in **Table S1c-S1g**.

Our paired T-test approach accounted for batch effects by design and restricted our candidate DEGs to those with a fold-difference in expression of >1.5 across ≥3 of 4 paired comparisons. This achieved our primary goal of identifying high-confidence cell-type specific markers and functional targets like *Ptger3*.

However, to identify DEGs less stringently (simply a significant *average* fold-change of 1.5), and to sidestep re-using samples in paired t-tests, we also performed intercept-free linear modeling analysis in R using the *limma* package on the same microarray data from the *Slc6a2*-LPS and *Slc6a4*-LPS experiments. The model was implemented using the following formula:

design <- model.matrix(~0+group+batch)

Where the group variable was coded as follows for the *Slc6a2* model (and analogously for the *Slc6a4* model):

sample_id	cell_type	treat	trap	sex	Batch	group
A2.P.F.IP_A1	SLC6A2	PBS	T	F	B	PBS_F_T
A2.P.F.IP_C3	SLC6A2	PBS	T	F	A	PBS_F_T
A2.P.M.IP_A3	SLC6A2	PBS	T	M	B	PBS_M_T
A2.P.M.IP_A5	SLC6A2	PBS	T	M	A	PBS_M_T
A2.L.F.IP_A2	SLC6A2	LPS	T	F	B	LPS_F_T
A2.L.F.IP_A6	SLC6A2	LPS	T	F	A	LPS_F_T
A2.L.M.IP_A4	SLC6A2	LPS	T	M	A	LPS_M_T
A2.L.M.IP_C1	SLC6A2	LPS	T	M	B	LPS_M_T
A2.P.F.PRE_D6	SLC6A2	PBS	P	F	A	PBS_F_P
A2.P.F.UB_D1	SLC6A2	PBS	P	F	B	PBS_F_P
A2.P.M.PRE_D4	SLC6A2	PBS	P	M	A	PBS_M_P
A2.P.M.UB_D3	SLC6A2	PBS	P	M	B	PBS_M_P
A2.L.F.PRE_D5	SLC6A2	LPS	P	F	A	LPS_F_P
A2.L.F.UB_D2	SLC6A2	LPS	P	F	B	LPS_F_P
A2.L.M.UB_F1	SLC6A2	LPS	P	M	B	LPS_M_P

The desired comparisons were made between groups using the following contrasts:

MvF_Trap = (PBS_M_T + LPS_M_T)/2 - (PBS_F_T + LPS_F_T)/2
LPSvPBS_Trap = (LPS_M_T + LPS_F_T)/2 - (PBS_M_T + PBS_F_T)/2
MvF_Pre = (PBS_M_P + LPS_M_P)/2 - (PBS_F_P + LPS_F_P)/2
LPSvPBS_Pre = (LPS_M_P + LPS_F_P)/2 - (PBS_M_P + PBS_F_P)/2
TrapvPre_M = (PBS_M_T + LPS_M_T)/2 - (PBS_M_P + LPS_M_P)/2
TrapvPre_F = (PBS_F_T + LPS_F_T)/2 - (PBS_F_P + LPS_F_P)/2
TrapvPre_LPS = (LPS_M_T + LPS_F_T)/2 - (LPS_M_P + LPS_F_P)/2
TrapvPre_PBS = (PBS_M_T + PBS_F_T)/2 - (PBS_M_P + PBS_F_P)/2

Note that for assessing main effects of sex or LPS, the available *n* of LC TRAP samples was 4. We did not examine interaction effects for lack of statistical power (*n=2* for the cross-comparison). For *Slc6a2* mice, this analysis

revealed 277 genes with sex-differential upregulation in male *Slc6a2* cells and 304 genes with sex-differential upregulation in female *Slc6a2* cells (including >85% of those from analysis above). This was still substantially higher than the sex-differentially upregulated gene sets from *Slc6a4* mice (15 genes in male, 15 genes in female). Resulting *p*-values from the latter analytical approach for genes passing differential expression criteria of the former approach are included in **Table S1c-S1g**. Fold changes and *p*-values from the *limma* analysis for the entire the entire array probeset are in **Table S3**.

Motif Analysis of peri-TSS Sequences of Sex-DEGs in LC: sequence acquisition and exon masking. For each sex-differentially expressed gene identified in the LC (**Table S1f,g**), mm10 genomic coordinates covering 10kb 5' and 10kb 3' to the canonical TSS were acquired from UCSC genome browser. For genes with multiple transcripts, the TSS of the longest transcript was selected. To perform motif discovery strictly within noncoding DNA sequences, the coordinates of all exon sequences in each range were acquired from UCSC. The mm10 genome was hard-masked (e.g., C->N) within all exon coordinates using *bedtools maskfasta*. The FASTA sequences for the 20kb regions were then extracted from the exon-masked genome using *bedtools getfasta*.

Conservation scoring and masking prior to MEME. For each base over 20kb regions, PhyloP scores—quantifying sequence conservation among placental mammals—were retrieved from UCSC**.** The threshold for defining conservation was a PhyloP score of 0.28, determined by counting the number of bases exceeding a score in steps of 0.01 and finding the step giving the greatest decrease in number of suprathreshold bases; this score corresponded to approximately 25% of input bases. Finally, to smooth the data, we used a "sliding mean" algorithm, acquiring the mean PhyloP score 15bp upstream and 15bp downstream of each base, with a step size of 1. Bases falling within ≥ 1 31bp window with a suprathreshold mean conservation score were retained; all others were hard-masked within the existing exon-masked sequences.

MEME analysis. Masked sequence sets for the male-enriched and female-enriched genes were then submitted to MEME (Bailey et al., 2015) for *de novo* motif analysis for motifs ranging 8-20bp in size. Two analyses were performed: one using the –zoops setting, which assumes and detects no more than one instance of a motif in each input sequence, and another using the –anr setting, which allows detection of multiple repeats of a motif within a given input sequence. The former allows us to detect how many sequences contain a given motif, while the latter allows us to detect how many total occurrences of a motif were found. MEME returns E-values, a built-in calculation of the likelihood of a motif occurring as many times as observed compared to a MEME-generated scrambled version of the input sequence. In the third "discriminative" analysis, one sex's sequence set was submitted as input and the other's as control, wherein E-scores represent the comparison between the input and "control" set, as opposed to input vs. scrambled. "Discriminative mode" in MEME only allows use of the –zoops algorithm; therefore, -anr data could not be collected for the direct sequence comparisons. For identification of putative TF binding sites represented by these motifs, we submitted the motifs from MEME to another MEME suite tool, TomTom, comparing those motifs to known murine and vertebrate TF binding sites (Kulakovskiy et al., 2018; Mathelier et al., 2016; Weirauch et al., 2014).

Chi-square analysis of motif-containing genes in LC sex-enriched sets vs background. To assess whether the abundance of these motifs near sex-differentially expressed LC transcripts differed from the genome on the whole, 1000 random protein-coding TSSes were selected for generation and masking of analogous 20kb windows using the same pipeline. These sequences were searched for matches to the discovered motifs using FIMO at the same *p* cutoff for a "match" used during motif discovery. The number of unique genes in the background set containing ≥ 1 occurrence of the motif was then counted and compared to the sex-differential gene set using chi-square analysis, followed by Benjamani-Hochberg correction for twelve tests (one per motif).

Electrophysiology of LC neurons exposed to PTGER3 agonist/antagonist. Horizontal brain slices were obtained from deeply anesthetized 6-7 week old male and female C57/BL6J mice (*Jackson Laboratories*) containing the LC (240 μM), as described (Courtney and Ford, 2014). Briefly, brain slices were cut using a Vibratome (Leica) in warm (~30°C) artificial cerebral-spinal fluid (aCSF) solution containing (in mM): 126 NaCl, 2.5 KCl, 1.2 $MgCl_2$, 2.5 $CaCl_2$, 1.2 NaH_2PO_4, 21.4 $NaHCO_3$, and 11.1 D-glucose bubbled with 95% O_2 and 5% CO_2. Slices were incubated at 35°C for at least 45 minutes prior to use. MK-801 (10 μM) was included during the incubation to block NMDA receptors. Following incubation, slices were transferred to a recording chamber and constantly perfused at 2 ml/min with oxygenated aCSF warmed to 34 ± 2°C. Slices were visualized with a BX51WI microscope (Olympus) with custom-built infrared gradient contrast optics.

Whole-cell recordings were made using an Axopatch 200B amplifier (*Molecular Devices*). Patch pipettes (2.0-2.5 MΩ) were pulled from borosilicate glass (*World Precision Instruments*). For voltage clamp experiments the pipette internal solution contained (in mM): 115 K-methylsulphate, 20 NaCl, 1.5 $MgCl_2$, 10 K-HEPES, 10 BAPTA-tetrapotassium, 2 ATP, 0.3 GTP, and 6 sodium phosphocreatine; pH 7.4; 275 mOsm. LC neurons were held at a voltage of -60 mV. No series resistance compensation was used, and cells were discarded if their series resistance exceeded 15 MΩ. For current clamp experiments the pipette internal solution contained (in mM): 135 D-gluconate (K), 10 HEPES (K), 0.1 $CaCl_2$, 2 $MgCl_2$, 0.1 EGTA, 1 mg/mL ATP, 0.1 mg/mL GTP, and 1.5 mg/mL phosphocreatine, pH 7.4, 275 mOsm. Liquid junction potentials were not corrected. All recordings were acquired using an ITC-18 interface (*Instrutech*) and Axograph X (*Axograph Scientific*) at 5 kHz and filtered to 2 kHz. For presentation, long chart recordings were made using a Powerlab 4/20 and LabChart (*AD Instruments*). Data was sampled for presentation at 400 Hz. The LC was identified by its location between the mesencephalic tract motor neurons and the 4th ventricle and neurons were identified by a capacitance > 40 pF, an input resistance < 100 MΩ, and a tonic firing rate of 0.5 – 4 Hz. Examination of the current-voltage relationship of the sulprostone-evoked outward current revealed inward rectification and a hyperpolarized reversal potential (-120 mV).

Stereotaxic cannulation of LC. Adult male and female C57BL/6J mice (8-10 weeks) were group-housed, given *ad libitum* access to food pellets and water and maintained on a 12/12 hour light:dark cycle (lights on at 6:00 AM). For surgery, mice were anesthetized in an induction chamber (4% isoflurane), then placed in a stereotaxic frame (*Kopf Instruments, Model 1900*) where they were maintained at 1-2% isoflurane. We performed craniotomies for insertion of two anchor screws and bilateral cannulae (*PlasticsOne, Inc*.). Cannulae were implanted above the LC (AP -5.45, ML +/-1.00, DV -3.00 mm relative to Bregma). Cannulae and anchor screws were then affixed to the skull using dental cement. Mice were allowed to recover for 7-9 days prior to behavioral testing. Animals were also habituated to handling and connection to pharmacological tubing for 3 consecutive days prior to behavioral testing.

Sulprostone and vehicle preparation for intracranial infusion. A 10.7mM (5mg/mL) stock solution of sulprostone in 200uL methyl acetate (*Tocris*) was diluted with an additional 800uL methyl acetate (*Sigma Aldrich*) to achieve a stock concentration of 1mg/mL. 1.12uL of this solution was then added to 12mL aCSF, achieving a final concentration of 200nM (the same concentration applied to *ex vivo* LC slices). 1.12uL of methyl acetate was added to 12mL aCSF for the vehicle-only controls.

Stress-induced anxiety behavioral paradigm. Mice were intracranially infused via bilateral cannulae with either sulprostone (0.4 µL per side, delivering 3.72pg sulprostone per side for drug condition) or its vehicle at a rate of 0.2 µL/min. Immediately following infusion, all mice were restrained for 30 minutes in 50 mL plastic conical tubes with drilled holes permitting air circulation and allowing the tail to extend beyond the tube (adapted from (McCall et al., 2015)). Immediately following restraint stress, animals were transferred to the open field for a 20-minute test. The open field testing (OFT) was performed in a rectangular enclosure 59x39 cm within a sound attenuated enclosure with lighting measured and maintained at ~25 lux. The open field was cleaned with 70% ethanol between each trial. Mice were returned to their home cage for 50 minutes after OFT; 10 minutes later (60min after the end of OFT), isoflurane anesthesia was administered prior to paraformaldehyde perfusion and brain dissection (as previously described). For the no-drug (stress vs. no-stress only, **Figure 4E-4H**), no surgeries or intracranial infusions were performed, and this same protocol was used beginning with the 30 minutes of restraint. Anymaze was used for video recording of animal movements for center and periphery analysis. The center zone was defined as a concentric rectangle comprised of 50% the total area of the OFT arena. Time and frequency in the center was used as a measure of anxiety-like behavior. Cannula placement was confirmed by cryostat sectioning of perfused brains to determine mice for inclusion in the final behavioral and c-FOS analyses.

c-FOS quantification in LC following sulprostone/vehicle, restraint, and OFT. Following behavior, perfusion, and slicing, 40µm sections of brain containing LC were subjected to immunohistochemistry for phospho-Ser32 c-Fos and TH (n=5 vehicle treated males, 5 vehicle-treated females, 4 sulprostone-treated males, 6 sulprostone-treated females; see methods described under *Immunohistochemistry*). Antibodies are described in **Table S1j**. All sections were imaged on a Zeiss AxioScan.Z1 microscope (Karl Zeiss, Germany). Gain, light intensity, and exposure time were identical for all prepared microscope slides. All images were processed with the same settings using ImageJ: background was first subtracted from the images, ROIs were made around the LC as determined by TH expression, and average pixel intensity was measured. Additionally, the number of Fos-expressing and TH-expressing cells were counted manually by an experimenter blind to treatment groups.

Estrous staging of female mice after OFT paradigm. In order to assess whether estrous stages and their corresponding hormonal milieus influenced baseline or sulprostone-moderated behaviors, vaginal cytology was

performed after female mice were anesthetized, but before perfusion began. Cytology was performed using 100uL H2O to perform vaginal lavage, followed by cresyl violet staining of the dried smear as previously described (McLean et al., 2012). Estrous stage was assessed as proestrous, estrous, metestrous, or diestrous by light microscopy based on cell types and structures (Byers et al., 2012; McLean et al., 2012).

Supplemental References:

Austin, M.C., Cottingham, S.L., Paul, S.M., and Crawley, J.N. (1990). Tyrosine hydroxylase and galanin mRNA levels in locus coeruleus neurons are increased following reserpine administration. Synapse *6*, 351–357.

Bacopoulos, N.G., and Bhatnagar, R.K. (1977). Correlation between tyrosine hydroxylase activity and catecholamine concentration or turnover in brain regions. J. Neurochem. *29*, 639–643.

Bailey, T.L., Johnson, J., Grant, C.E., and Noble, W.S. (2015). The MEME Suite. Nucleic Acids Res. *43*, W39–49.

Byers, S.L., Wiles, M.V., Dunn, S.L., and Taft, R.A. (2012). Mouse Estrous Cycle Identification Tool and Images. PLOS ONE *7*, e35538.

Chai, Z., Gatti, S., Toniatti, C., Poli, V., and Bartfai, T. (1996). Interleukin (IL)-6 gene expression in the central nervous system is necessary for fever response to lipopolysaccharide or IL-1 beta: a study on IL-6-deficient mice. J. Exp. Med. *183*, 311–316.

Courtney, N.A., and Ford, C.P. (2014). The Timing of Dopamine- and Noradrenaline-Mediated Transmission Reflects Underlying Differences in the Extent of Spillover and Pooling. J. Neurosci. *34*, 7645–7656.

Dalal, J., Roh, J.H., Maloney, S.E., Akuffo, A., Shah, S., Yuan, H., Wamsley, B., Jones, W.B., Strong, C. de G., Gray, P.A., et al. (2013). Translational profiling of hypocretin neurons identifies candidate molecules for sleep regulation. Genes Dev. *27*, 565–578.

Dennis, G., Sherman, B.T., Hosack, D.A., Yang, J., Gao, W., Lane, H.C., and Lempicki, R.A. (2003). DAVID: Database for Annotation, Visualization, and Integrated Discovery. Genome Biol. *4*, R60.

Dougherty, J.D., Schmidt, E.F., Nakajima, M., and Heintz, N. (2010). Analytical approaches to RNA profiling data for the identification of genes enriched in specific cells. Nucleic Acids Res. *38*, 4218–4230.

Dougherty, J.D., Maloney, S.E., Wozniak, D.F., Rieger, M.A., Sonnenblick, L., Coppola, G., Mahieu, N.G., Zhang, J., Cai, J., Patti, G.J., et al. (2013). The disruption of Celf6, a gene identified by translational profiling of serotonergic neurons, results in autism-related behaviors. J. Neurosci. Off. J. Soc. Neurosci. *33*, 2732–2753.

Doyle, J.P., Dougherty, J.D., Heiman, M., Schmidt, E.F., Stevens, T.R., Ma, G., Bupp, S., Shrestha, P., Shah, R.D., Doughty, M.L., et al. (2008). Application of a Translational Profiling Approach for the Comparative Analysis of CNS Cell Types. Cell *135*, 749–762.

Gordon, C. (1993). Temperature Regulation in Laboratory Rodents (Cambridge University Press).

Görlich, A., Antolin-Fontes, B., Ables, J.L., Frahm, S., Slimak, M.A., Dougherty, J.D., and Ibañez-Tallon, I. (2013). Reexposure to nicotine during withdrawal increases the pacemaking activity of cholinergic habenular neurons. Proc. Natl. Acad. Sci. U. S. A. *110*, 17077–17082.

Hasegawa, Y., Hida, T., and Arai, R. (1999). Noradrenaline-degrading activity of monoamine oxidase is localized in noradrenergic neurons of the locus coeruleus of the rat. Neurosci. Lett. *264*, 61–64.

Heiman, M., Kulicke, R., Fenster, R.J., Greengard, P., and Heintz, N. (2014). Cell type–specific mRNA purification by translating ribosome affinity purification (TRAP). Nat. Protoc. *9*, 1282–1291.

Kozak, W., Kluger, M.J., Soszynski, D., Conn, C.A., Rudolph, K., Leon, L.R., and Zheng, H. (1998). IL-6 and IL-1 beta in fever. Studies using cytokine-deficient (knockout) mice. Ann. N. Y. Acad. Sci. *856*, 33–47.

Kulakovskiy, I.V., Vorontsov, I.E., Yevshin, I.S., Sharipov, R.N., Fedorova, A.D., Rumynskiy, E.I., Medvedeva, Y.A., Magana-Mora, A., Bajic, V.B., Papatsenko, D.A., et al. (2018). HOCOMOCO: towards a complete collection of transcription factor binding models for human and mouse via large-scale ChIP-Seq analysis. Nucleic Acids Res. *46*, D252–D259.

Leon, L.R. (2002). Invited Review: Cytokine regulation of fever: studies using gene knockout mice. J. Appl. Physiol. *92*, 2648–2655.

Mathelier, A., Fornes, O., Arenillas, D.J., Chen, C.-Y., Denay, G., Lee, J., Shi, W., Shyr, C., Tan, G., Worsley-Hunt, R., et al. (2016). JASPAR 2016: a major expansion and update of the open-access database of transcription factor binding profiles. Nucleic Acids Res. *44*, D110-5.

McCall, J.G., Al-Hasani, R., Siuda, E.R., Hong, D.Y., Norris, A.J., Ford, C.P., and Bruchas, M.R. (2015). CRH Engagement of the Locus Coeruleus Noradrenergic System Mediates Stress-Induced Anxiety. Neuron *87*, 605–620.

McLean, A.C., Valenzuela, N., Fai, S., and Bennett, S.A.L. (2012). Performing vaginal lavage, crystal violet staining, and vaginal cytological evaluation for mouse estrous cycle staging identification. J. Vis. Exp. JoVE e4389–e4389.

Melander, T., Hökfelt, T., Rökaeus, A., Cuello, A.C., Oertel, W.H., Verhofstad, A., and Goldstein, M. (1986). Coexistence of galanin-like immunoreactivity with catecholamines, 5-hydroxytryptamine, GABA and neuropeptides in the rat CNS. J. Neurosci. *6*, 3640–3654.

Morin, X., Cremer, H., Hirsch, M.R., Kapur, R.P., Goridis, C., and Brunet, J.F. (1997). Defects in sensory and autonomic ganglia and absence of locus coeruleus in mice deficient for the homeobox gene Phox2a. Neuron *18*, 411–423.

Schroeter, S., Apparsundaram, S., Wiley, R.G., Miner, L.H., Sesack, S.R., and Blakely, R.D. (2000). Immunolocalization of the cocaine- and antidepressant-sensitive l-norepinephrine transporter. J. Comp. Neurol. *420*, 211–232.

Silva, A.F., Sousa, D.S., Medeiros, A.M., Macêdo, P.T., Leão, A.H., Ribeiro, A.M., Izídio, G.S., and Silva, R.H. (2016). Sex and Estrous Cycle Influence Diazepam Effects on Anxiety and Memory: Possible Role of Progesterone. Prog. Neuropsychopharmacol. Biol. Psychiatry *70*, 68–76.

Swanson, L.W., and Hartman, B.K. (1975). The central adrenergic system. An immunofluorescence study of the location of cell bodies and their efferent connections in the rat utilizing dopamine-B-hydroxylase as a marker. J. Comp. Neurol. *163*, 467–505.

Weihe, E., Depboylu, C., Schütz, B., Schäfer, M.K.-H., and Eiden, L.E. (2006). Three types of tyrosine hydroxylase-positive CNS neurons distinguished by dopa decarboxylase and VMAT2 co-expression. Cell. Mol. Neurobiol. *26*, 659–678.

Weirauch, M.T., Yang, A., Albu, M., Cote, A.G., Montenegro-Montero, A., Drewe, P., Najafabadi, H.S., Lambert, S.A., Mann, I., Cook, K., et al. (2014). Determination and Inference of Eukaryotic Transcription Factor Sequence Specificity. Cell *158*, 1431–1443.

Xu, X., Wells, A.B., O'Brien, D.R., Nehorai, A., and Dougherty, J.D. (2014). Cell type-specific expression analysis to identify putative cellular mechanisms for neurogenetic disorders. J. Neurosci. Off. J. Soc. Neurosci. *34*, 1420–1431.